Proceedings of the
Annual Stability Conference
Structural Stability Research Council
Charlotte, North Carolina, April 11-14, 2023

Modeling partially yielded regions of W-Shapes using a second-order stiffness reduction over the element length

Naomi R. Silva[1], Barry T. Rosson[2]

Abstract

Stiffness reduction occurs due to yielding of the cross-section of W-Shapes under certain conditions of residual stress, moment, and axial load. This paper investigates the development and performance of a new closed-form stiffness matrix for a beam element that assumes a second-order stiffness reduction over the partially yielded regions of W-Shapes. Even though it is well known the stiffness reduction is nonlinear when the moments vary over the partially yielded regions, it is common to use a stiffness matrix that is based on an assumed linear stiffness reduction. To evaluate the performance of the new stiffness matrix, two beams and three unbraced frames were analyzed using MASTAN2 considering five load increment sizes and nine element conditions. Discussion and recommendations are provided regarding the parameters that influence the modeling results and the ability of the new stiffness matrix to provide better results than the current stiffness matrix that assumes a linear stiffness reduction.

1. Introduction

Three-dimensional m-p-τ surface plots have been used to develop an empirical inelastic material model for use in a closed-form stiffness matrix that assumes a linear stiffness variation over the beam element length (Zeimian and McGuire 2002). Since stiffness reduction is known to vary nonlinearly over the partially yielded regions of steel members, even for linearly varying moment conditions, there is a need to develop and evaluate a similarly derived closed-form stiffness matrix that assumes a second-order stiffness variation over the element length. For structures with nonlinear material and geometric behavior, the load increment size and the number of elements used to model each member can have a profound effect on the accuracy of the modeling results (Zubydan 2011; Rosson 2018).

This paper focuses on the development and performance of a closed-form stiffness matrix that assumes a second-order stiffness reduction over the element length. Its performance was evaluated by analyzing two test beams and three benchmark frames with loads near the collapse condition of each structure. Finite element model analyses were conducted using MASTAN2 (Ziemian and McGuire 2015) with closed-form stiffness matrices that were developed based on a first-order or second-order stiffness reduction over the element length. Since the load increment

[1] Former Graduate Student, Florida Atlantic University, <silvan2016@fau.edu>
[2] Professor, Florida Atlantic University, <rosson@fau.edu>

size and the number of elements used to model each member also influences the modeling accuracy, the performance comparisons of the two stiffness matrices included these effects. The ability of the second-order stiffness matrix to consistently provide better results than the first-order stiffness matrix was evaluated, and conclusions were made as to its recommended use when modeling the yielded regions of W-Shapes.

2. Stiffness Reduction Model

Much research has been done on developing improved empirical relationships to account for stiffness reduction that occurs due to yielding in structural steel members. The stiffness reduction of compact W-Shapes with an ECCS residual stress pattern was studied in detail using a fiber element model with over 2,000 elements (Rosson 2019).

As demonstrated in Rosson (2018), the boundary at which there is no stiffness reduction ($\tau = 1$) is found when the maximum residual stress, flexural stress, and axial stress sum to σ_y. The maximum normalized moment (M_1 / M_p) at which $\tau = 1$ is maintained for major-axis bending is given as

$$m_1 = \frac{S_x}{Z_x}(1 - c_r - p) \tag{1}$$

where S_x is the major-axis elastic section modulus, Z_x is the major-axis plastic section modulus, c_r is the residual stress ratio (σ_r / σ_y), and p is the normalized axial load (P / P_y). The sign on the yield load P_y matches that of P such that p is always positive. Since this equation is based only on the accumulation of compression stresses at the end of each flange, the actual shape of the residual pattern does not affect the equation provided the maximum residual compression stress σ_r occurs at the end of the flanges (Rosson 2018).

To determine the stiffness reduction τ for a given p and c_r condition, the major-axis moment of inertia of the remaining cross-section that has not yielded is divided by the original major-axis moment of inertia I_x. The stiffness reduction τ for the major-axis condition is found to be

$$\tau_p = \frac{\lambda\lambda_1^2\left[1 - \left(1 - \sqrt{\frac{1-p}{c_r}}\right)^3\right] + \sqrt{\frac{1-p}{c_r}}\left[2 + 6(1+\lambda_1)^2\right]}{\lambda\lambda_1^2 + 2 + 6(1+\lambda_1)^2} \tag{2}$$

where $\lambda = A_w/A_f$, $\lambda_o = t_w/b_f$, and $\lambda_1 = d_w/t_f$ (Rosson 2017).

Two equations are needed to determine the m and p conditions when $\tau = 0$. For major-axis bending with axial compression condition, one equation is needed when the plastic neutral axis is outside the flange thickness, and the other is needed when it is inside the flange thickness. Eqs. 3 and 4 do not depend upon the shape of the residual stress pattern.

$$when\ p < \frac{\lambda}{2+\lambda} \qquad m_0 = 1 - \frac{p^2(2+\lambda)^2}{4\lambda_o + \lambda(4+\lambda)} \tag{3}$$

$$when\ p \geq \frac{\lambda}{2+\lambda} \qquad m_0 = \frac{(2+\lambda_1)^2 - [p(2+\lambda) - \lambda + \lambda_1]^2}{4 + \lambda_1(4+\lambda)} \tag{4}$$

The inelastic material model given in Eqs. 5 and 6 uses the closed-form equations for the perimeter conditions m_1, τ_p and m_0 in Fig. 1.

$$when\ p < 1 - c_r \qquad \tau = 1 - \left(\frac{m - m_1}{m_0 - m_1}\right)^n \tag{5}$$

$$when\ p \geq 1 - c_r \qquad \tau = \tau_p \left[1 - \left(\frac{m}{m_0}\right)^n\right] \tag{6}$$

where n is a constant that varies depending on the axis of bending. For a given m, p and c_r condition, the stiffness can be evaluated from the m_1, τ_p and m_0 values from Eqs. 1, 2, 3 and 4. The ability of Eqs. 5 and 6 to approximate the m-p-τ surface conditions are shown in Fig. 1 with a c_r = 0.3 and n = 8 under major-axis bending conditions.

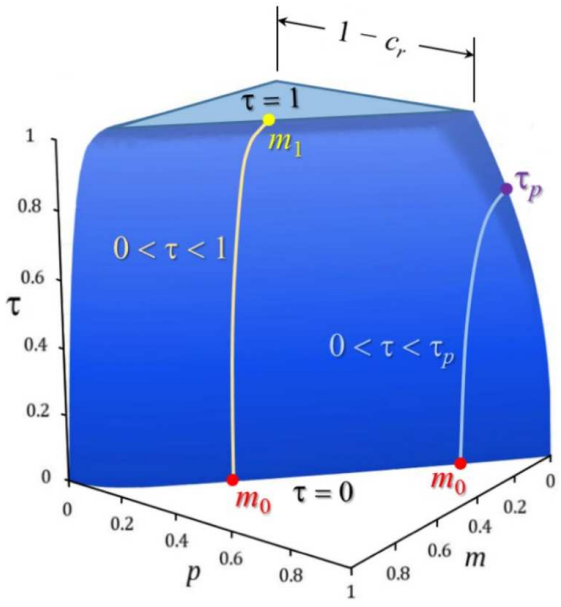

Figure 1: Major-axis bending m-p-τ surface plot with c_r = 0.3 and n = 8

3. New Stiffness Matrix

Since bending moments often vary along the length of beam-columns, the nonlinear stiffness reduction in the yielded regions must be accounted for. As given in Eq. 7, the tangent modulus is assumed to vary as a second-order polynomial over the element length.

$$E(x) = \left(\frac{2x^2}{L^2} - \frac{3x}{L} + 1\right)a + \left(\frac{4x}{L} - \frac{4x^2}{L^2}\right)c + \left(\frac{2x^2}{L^2} - \frac{x}{L}\right)b \tag{7}$$

where a, b, and c are the τ values based on the m and p condition at the start, end, and middle of the element, respectively. The m and p conditions at the middle can be easily evaluated based on equilibrium with the member end forces and applied loads. The shape functions are the same as those used to develop the beam element for an elastic, prismatic beam (McGuire *et al*. 2000).

$$\lfloor N' \rfloor = \left\lfloor \frac{6}{L^2}\left(\frac{2x}{L}-1\right) \quad \frac{2}{L}\left(\frac{3x}{L}-2\right) \quad \frac{6}{L^2}\left(1-\frac{2x}{L}\right) \quad \frac{2}{L}\left(\frac{3x}{L}-1\right) \right\rfloor \tag{8}$$

Using the tangent modulus expression in Eq. 7, the stiffness matrix terms were found by evaluating the following integral.

$$[k] = \int_0^L \{N'\}\left[\left(\frac{2x^2}{L^2}-\frac{3x}{L}+1\right)a + \left(\frac{4x}{L}-\frac{4x^2}{L^2}\right)c + \left(\frac{2x^2}{L^2}-\frac{x}{L}\right)b\right] EI_x \lfloor N' \rfloor dx \tag{9}$$

The integrations result in the following closed-form stiffness matrix $[k]$ for major-axis bending

$$\frac{EI_x}{L}\begin{bmatrix} \frac{12}{L^2}\left(\frac{3a+4c+3b}{10}\right) & \frac{6}{L}\left(\frac{7a+6c+2b}{15}\right) & -\frac{12}{L^2}\left(\frac{3a+4c+3b}{10}\right) & \frac{6}{L}\left(\frac{2a+6c+7b}{15}\right) \\ & 4\left(\frac{31a+28c+b}{60}\right) & -\frac{6}{L}\left(\frac{7a+6c+2b}{15}\right) & 2\left(\frac{11a+8c+11b}{30}\right) \\ & & \frac{12}{L^2}\left(\frac{3a+4c+3b}{10}\right) & -\frac{6}{L}\left(\frac{2a+6c+7b}{15}\right) \\ & Sym. & & 4\left(\frac{a+28c+31b}{60}\right) \end{bmatrix} \tag{10}$$

The stiffness matrix $[k]$ that assumes a linear variation of stiffness reduction over the element length is given in Eq. 11 (McGuire and Ziemian 2002).

$$\frac{EI_x}{L}\begin{bmatrix} \frac{12}{L^2}\left(\frac{a+b}{2}\right) & \frac{6}{L}\left(\frac{2a+b}{3}\right) & -\frac{12}{L^2}\left(\frac{a+b}{2}\right) & \frac{6}{L}\left(\frac{a+2b}{3}\right) \\ & 4\left(\frac{3a+b}{4}\right) & -\frac{6}{L}\left(\frac{2a+b}{3}\right) & 2\left(\frac{a+b}{2}\right) \\ & & \frac{12}{L^2}\left(\frac{a+b}{2}\right) & -\frac{6}{L}\left(\frac{a+2b}{3}\right) \\ & Sym. & & 4\left(\frac{a+3b}{4}\right) \end{bmatrix} \tag{11}$$

The beam element stiffness matrix in Eq. 10 will be referred to as the *abc* element in subsequent sections, and the stiffness matrix in Eq. 11 will be referred to as the *ab* element. Finite element analyses were conducted using MASTAN2 which allowed for geometric and material nonlinearities to be considered. Since the new stiffness matrix is not part of the MASTAN2 software, the stiffness matrix in Eq. 10 was added to the MATLAB source code. MASTAN2 contains an incremental analysis routine that easily allows for changing the load increment condition, and it also allows for easily subdividing the members into a specified number of elements.

4. Test Beam Models

Two test beams were used first to evaluate the performance of the *abc* element because geometric nonlinearities do not affect beam results as they tend to do with frames (Silva 2022). For each condition of load increment size and number of elements per member, the vertical deflection at a prescribed point on the beam was recorded. The exact conditions were modeled for each beam using the *ab* element and then again using the *abc* element. All models used a modulus of elasticity of 29,000 ksi and a yield stress of 50 ksi.

Test Beam 1 given in Fig. 2 is a W21x44 cantilevered beam with a concentrated moment M_1 and concentrated load Q_1. The length L is 180 inches. Using c_r = 0.3 and p = 0 in Eq. 1, yielding initiates over the full length of the beam with M_1 of 2,856 kip-in. The concentrated moment was applied first to initiate yielding, then the concentrated load Q_1 of 10.24 kips was applied to produce a moment of 4,700 k-in at the fixed-end. The darker blue region is closest to the plastic moment M_p of 4,770 kip-in. Deflection results were recorded at the free-end of the beam.

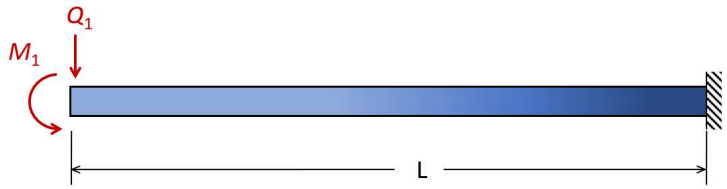

Figure 2: Test Beam 1 model and yielded region

Eq. 12 was used to determine the relative error of the deflection results and is given as

$$R.E._{deflection}\ (\%) = \frac{Approximate\ deflection\ -\ Exact\ deflection}{Exact\ deflection} \tag{12}$$

The "exact deflection" is determined from an analysis of Test Beam 1 using 9 *abc* elements equally spaced across the beam with 100 load increments. The "approximate deflection" is determined from an analysis using from 1 to 9 elements across the length of the beam with 10, 25, 50, 75, or 100 load increments. A "member" is defined to be the section between a support and a load, or between two adjacent loads. Test Beam 1 has one "member".

Comparing the results in Fig. 3 for the models using 1 element with 100 load increments, the *abc* element model has a relative error of +0.51%, and the *ab* element model has a relative error of +1.76%. Fig. 3 illustrates the effect that the number of load increments has on the relative error results. Reducing the number of load increments produces larger load increments sizes, and since the tangent stiffness coefficients are based on lower member forces from the previous load increment, the stiffness terms are overpredicted for each load increment and thus additional artificial stiffness accumulates over the full loading sequence. As the number of load increments decrease, the more the model is artificially stiffened. Considering first the models with only 1 element, both the *ab* and *abc* element models are less stiff than the "actual" stiffness; thus, the relative errors are positive but move downward due to artificial stiffening as the number of load increments decrease. It is noticed that artificial stiffening can produce deflections that are less than the "exact" deflections resulting in negative relative error results. The full range of results in Fig. 3 illustrates the need to carefully consider the number of elements and number of load

increments to use when performing an inelastic analysis. In general, the *abc* element provides superior results over the *ab* element, but a poor choice of load increments can eliminate its potential benefit. For instance, a model using 3 *abc* elements with 50 load increments gives an "exact" result, but when only 10 load increments are used the *abc* element gives a larger relative error than the *ab* element.

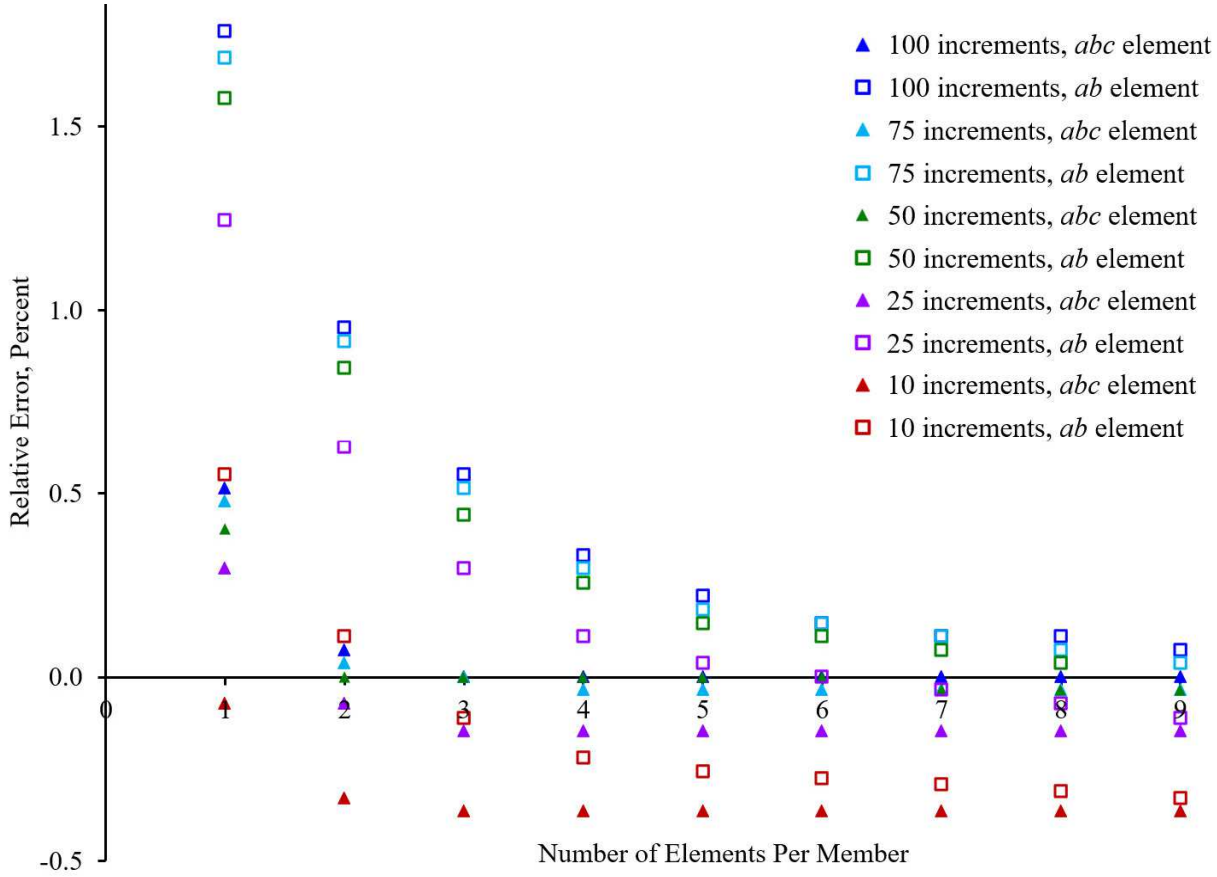

Figure 3: Test Beam 1 relative error results

Test Beam 2 given in Fig. 4 is a W18x50 two-span beam with concentrated loads Q_1 of 90 kips, Q_2 of 130 kips, and Q_3 of 85 kips. Q_1 and Q_3 are applied at mid-span, and Q_2 is applied at the quarter-point. The length L is 20 feet. The plastic moment M_p is 5,050 kip-in, and with all loads applied simultaneously, the maximum moment in the beam is 4,994 kip-in. Test Beam 2 has five "members". Deflections were recorded at the Q_3 location. The white regions are completely elastic, and the darker blue regions are closest to the plastic moment condition.

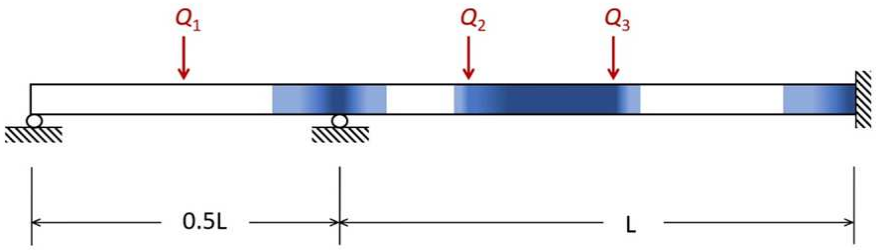

Figure 4: Test Beam 2 model and yielded regions

The results of the analyses for Test Beam 2 are given in Fig. 5 for all load increments and number of elements per member.

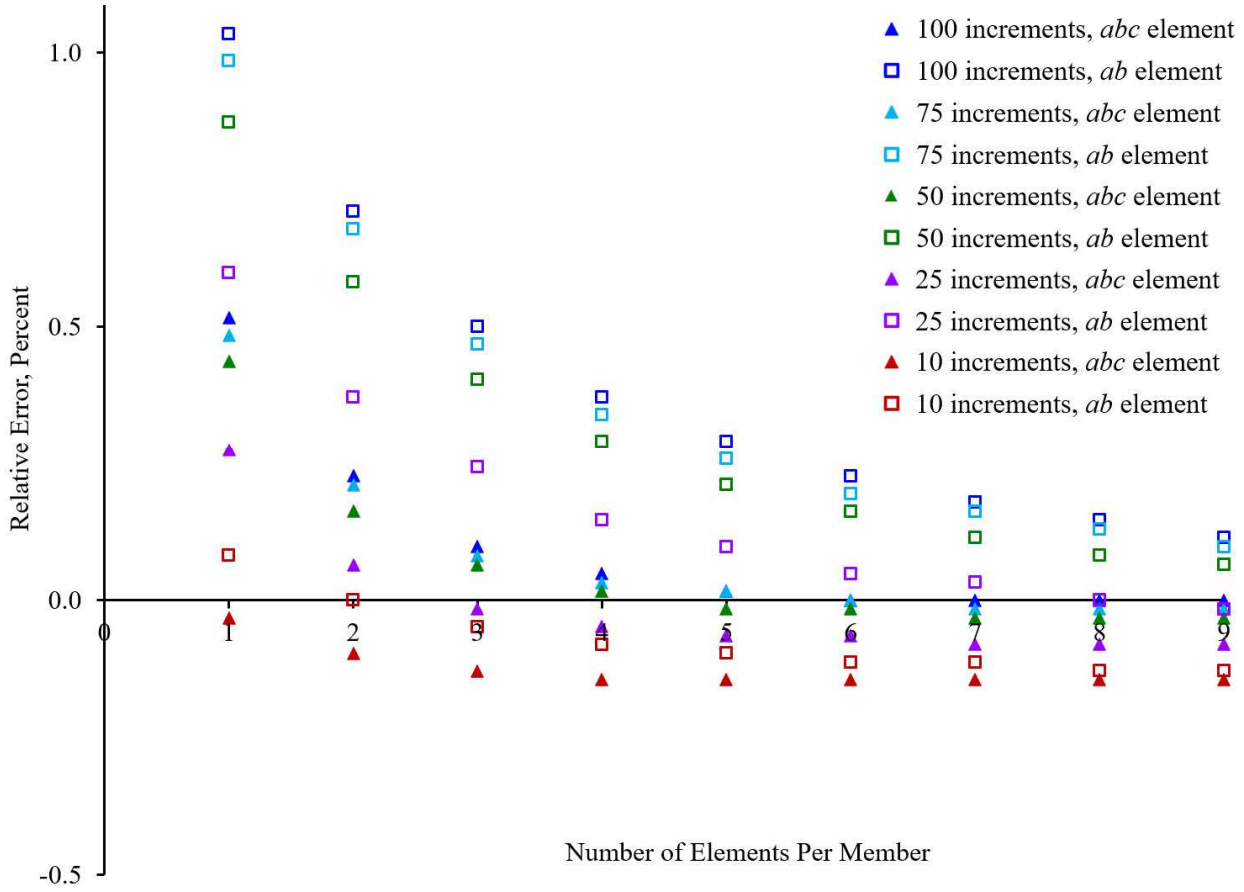

Figure 5: Test Beam 2 relative error results

Eq. 12 was used to determine the relative error of the deflection with the "exact" solution being that from the *abc* element model using 9 elements per member with 100 load increments. Comparing the models using 1 element per member with 100 load increments, the *abc* element model has a relative error of +0.51%, and the *ab* element model has a relative error of +1.03%. When the number of elements per member increases, the *abc* element model with 50 load increments gives results that are very near the "actual" stiffness condition of the beam when using 5 or more elements per member. Increasing the number of elements for the *ab* element model with 100 load increments improves the relative error, but error remains even up to 9 elements per member. Like the results for Test Beam 1, the relative error results for Test Beam 2 revealed the influence of artificial stiffness due to the increment size. In Fig. 5, as the load increment size increases, the relative errors move downward due to increased artificial stiffness. As with Test Beam 1, the artificial stiffness can produce negative relative error results for models with a low number of load increments. Without the benefit of having a complete picture of all the modeling results in Fig. 5, false conclusions can be made regarding the benefit of using the *abc* element. For example, the *ab* element model with 2 elements per member and 10 load increments gives an "exact" result, but the *abc* element model using the same modeling condition gives a small relative error.

5. Test Frame Models

Three test frames were used to evaluate the performance of the *abc* element in which geometric nonlinearities were allowed to affect the results (Silva 2022). For each load increment condition and number of elements per member, the horizontal deflection at the top of the frame was recorded. Initial geometric imperfections were modeled using an elastic critical load analysis, and the coordinates were updated based on the first eigenmode with an offset by $h/500$ in the direction of the lateral loads, where h is the total frame height in inches. All models used a modulus of elasticity of 29,000 ksi, a yield stress of 50 ksi, and all members were oriented with major-axis bending.

Test Frame 1 in Fig. 6 consists of three columns with hinge supports at the base and two beams with gravity and lateral loads applied at the joints. Table 1 summarizes the W-Shapes of the columns and beams, as well as the magnitude of the gravity and lateral loads. The length L is 26 feet. Test Frame 1 has six "members". In Fig. 6, yielding occurs in the left and middle columns due to the combination of high compression forces and large bending moments. The white regions are completely elastic, and the yielded regions are shaded in blue with the darker blue regions closest to the m_0 conditions given in Fig. 1.

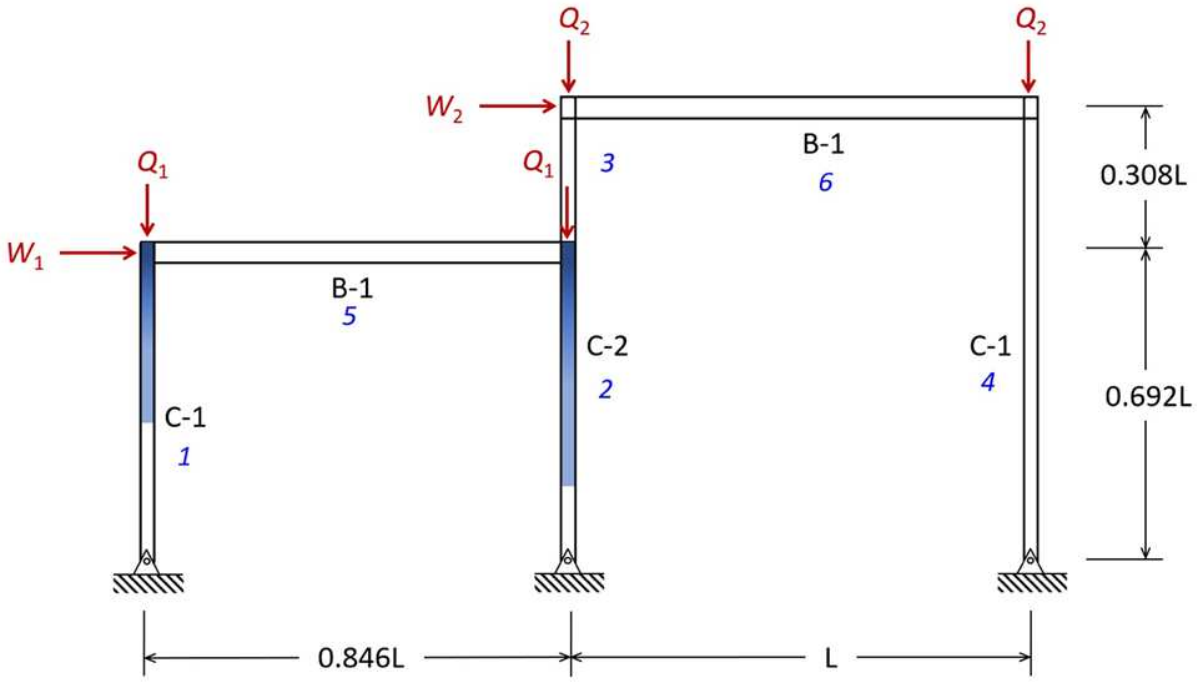

Figure 6: Test Frame 1 model and yielded regions

Table 1: Test Frame 1 member and load information

W-Shape		Gravity Loads (kips)		Lateral Loads (kips)	
B-1	W24x84	Q_1	110	W_1	11.52
C-1	W10x54	Q_2	130	W_2	7.68
C-2	W10x60				

In Fig. 7, the relative error of the displacements at the top level are given for the *ab* and *abc* element models where the number of elements per member varies from 2 to 10 with five different load increment conditions. The "exact" solution was taken to be the deflection from the *abc* element model using 10 elements per member with 100 load increments. The relative error results of Test Frame 1 are different than those of the test beams due primarily to the nonlinear geometric effects of the unbraced frame and the hinge supports. The column C-2 experiences a large interior bending moment due to significant P-δ effects from the axial loads Q_1 and Q_2. The overall frame also experiences a large P-Δ effect. The relative error results for the *abc* element models remain negative for all analysis conditions. This indicates the *abc* element models are stiffer than the *ab* element models with the *abc* element models experiencing lower nonlinear geometric effects and lower overall lateral deflections. Even though this indicates the *abc* element models are too stiff relative to the "actual" stiffness, the deflections increase as more elements are used in the model. Comparing the models using 2 elements per member with 100 load increments, the *abc* element model has a relative error of −1.00%, and the *ab* element model has a relative error of +3.21%. Maintaining 100 load increments and increasing the number of elements per member from 2 to 10 results in a convergence to the "exact" solution regardless the element type. As with the beam tests, decreasing the number of load increments artificially stiffens the modeled response and moves the relative errors downward.

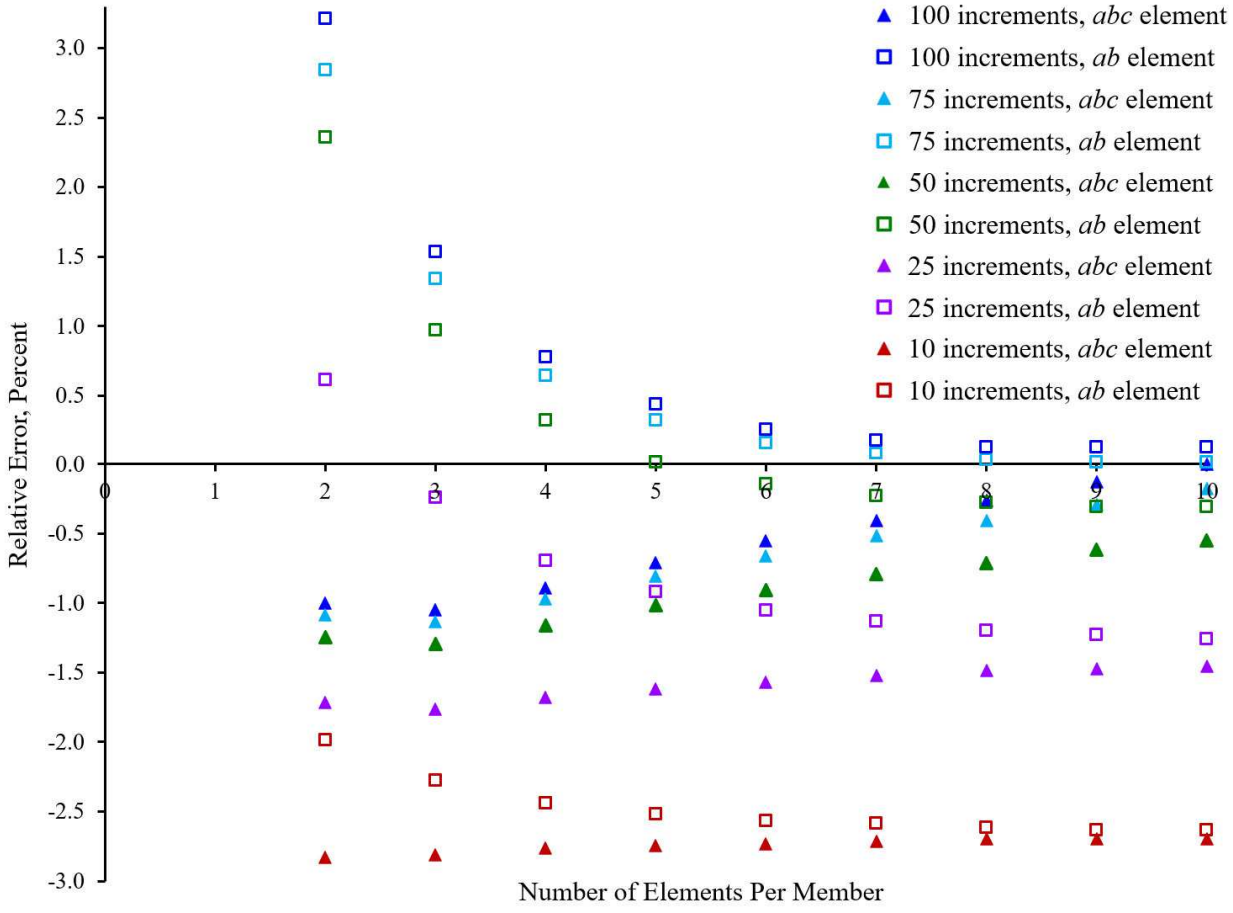

Figure 7: Test Frame 1 relative error results

Test Frame 2 in Fig. 8 is a three-story frame with a hinge support at the base of each column. Table 2 summarizes the W-Shapes of the columns and beams, as well as the magnitude of the gravity and lateral loads. Test Frame 2 has 21 "members". The length L is 30 feet.

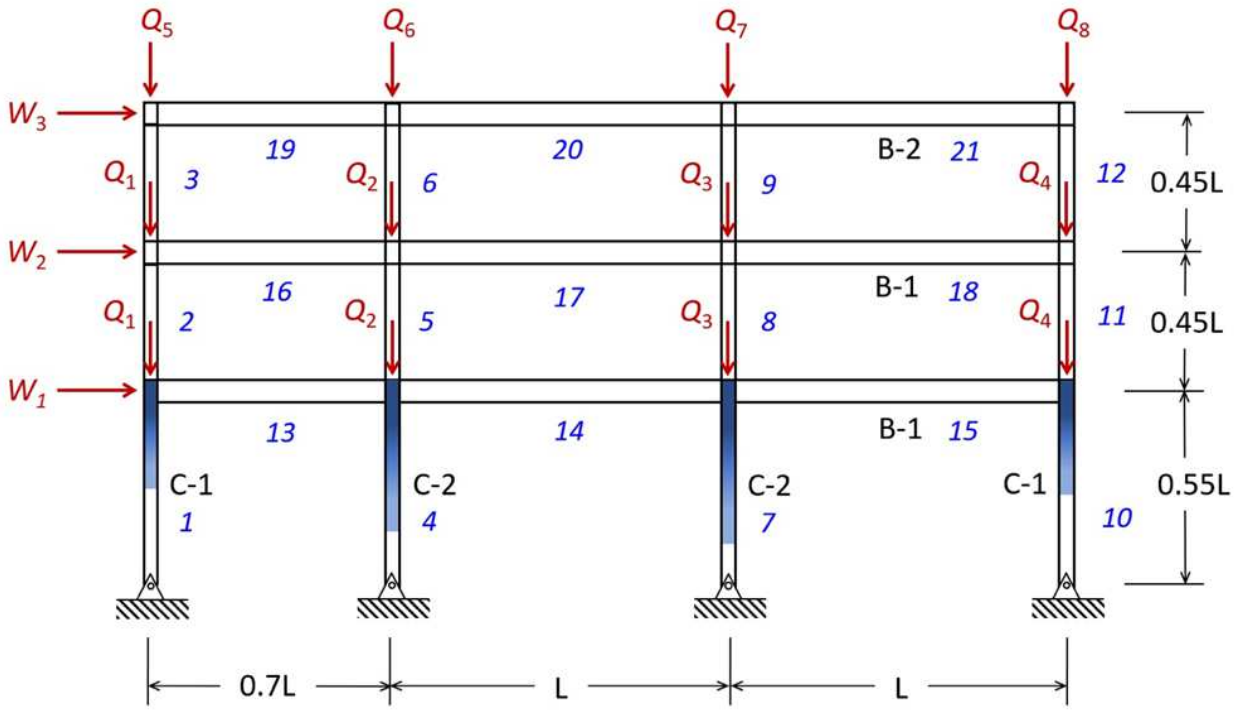

Figure 8: Test Frame 2 model and yielded regions

Table 2: Test Frame 2 member and load information

W-Shape		Gravity Loads (kips)				Lateral Loads (kips)	
B-1	W24x176	Q_1	94.5	Q_5	85.5	W_1	35.712
B-2	W24x162	Q_2	229.5	Q_6	207	W_2	44.64
C-1	W12x96	Q_3	270	Q_7	243	W_3	26.784
C-2	W14x145	Q_4	135	Q_8	121.5		

In Fig. 9, the relative error results of Test Frame 2 are very similar than those of Test Frame 1. This is due primarily to the nonlinear geometric effects of the unbraced frame and the hinge supports. The first-floor columns experience significant yielding in their upper sections due to the combination of high compression forces and large bending moments. Comparing the models using 2 elements per member with 100 load increments, the *abc* element model has a relative error of −1.12%, and the *ab* element model has a relative error of +2.90%. As with Test Frame 1, maintaining 100 load increments and increasing the number of elements per member from 2 to 10 results in a convergence to the "exact" solution regardless the element type. The deflection increases as more elements are used with the *abc* element models, and the deflection decreases as more elements are used with the *ab* element models. As with the other test structures, decreasing the number of load increments artificially stiffens the modeled response and moves the relative errors downward. Care must be taken in selecting the increment size and number of elements per member when modeling unbraced frames. For example, if only 10 load increments were used to determine the number of elements to use in the model, the accuracy only slightly improves with more *abc* elements and worsens with more *ab* elements; thus, an erroneous conclusion would be made that there is little to no benefit in using more elements, when in fact there is substantial benefit if more load increments are used.

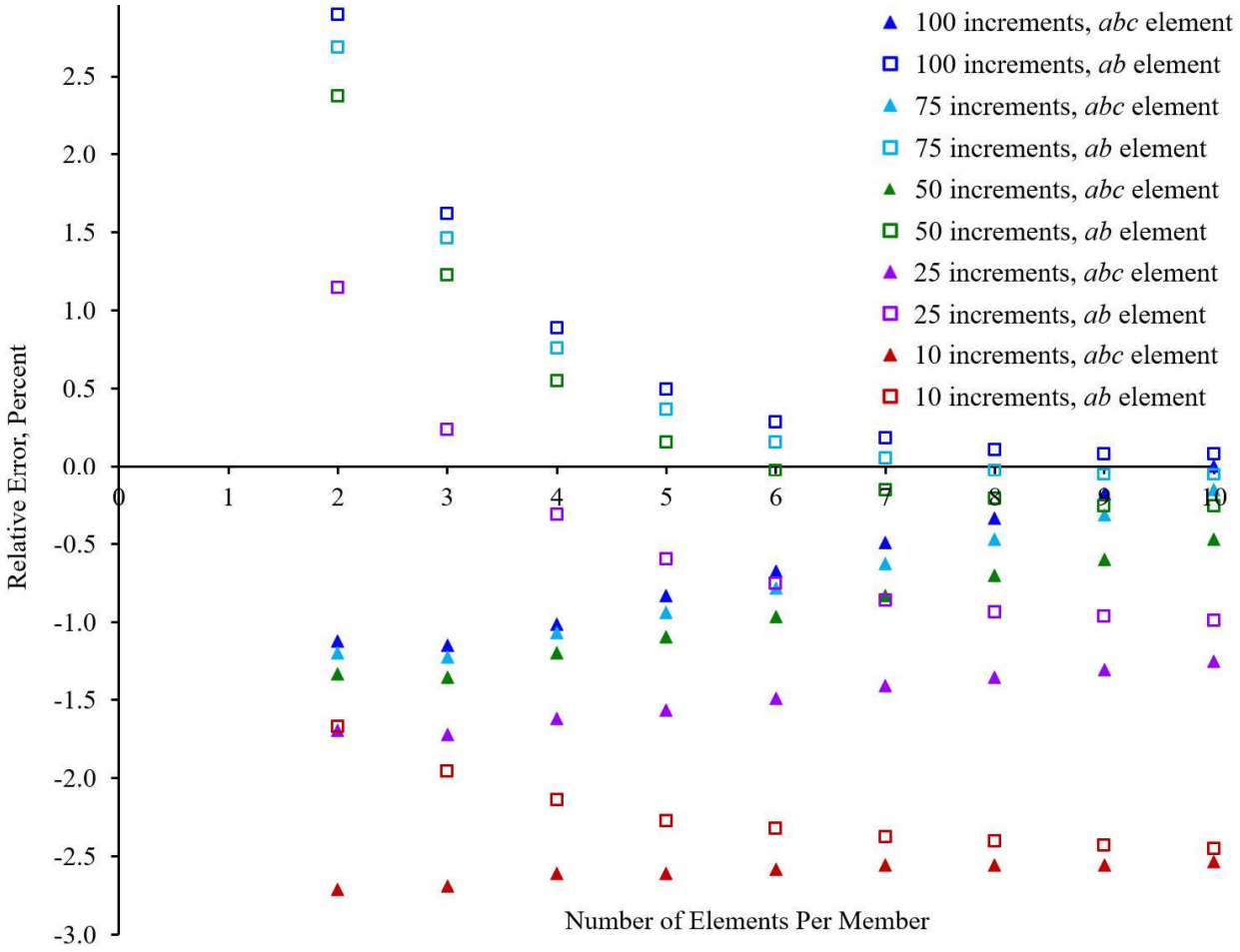

Figure 9: Test Frame 2 relative error results

Test Frame 3 in Fig. 10 is a six-story frame with a fixed support at the base of each column. Table 3 summarizes the W-Shapes of the columns and beams, as well as the magnitude of the gravity and lateral loads. Test Frame 3 has 30 "members". The length L is 30 feet.

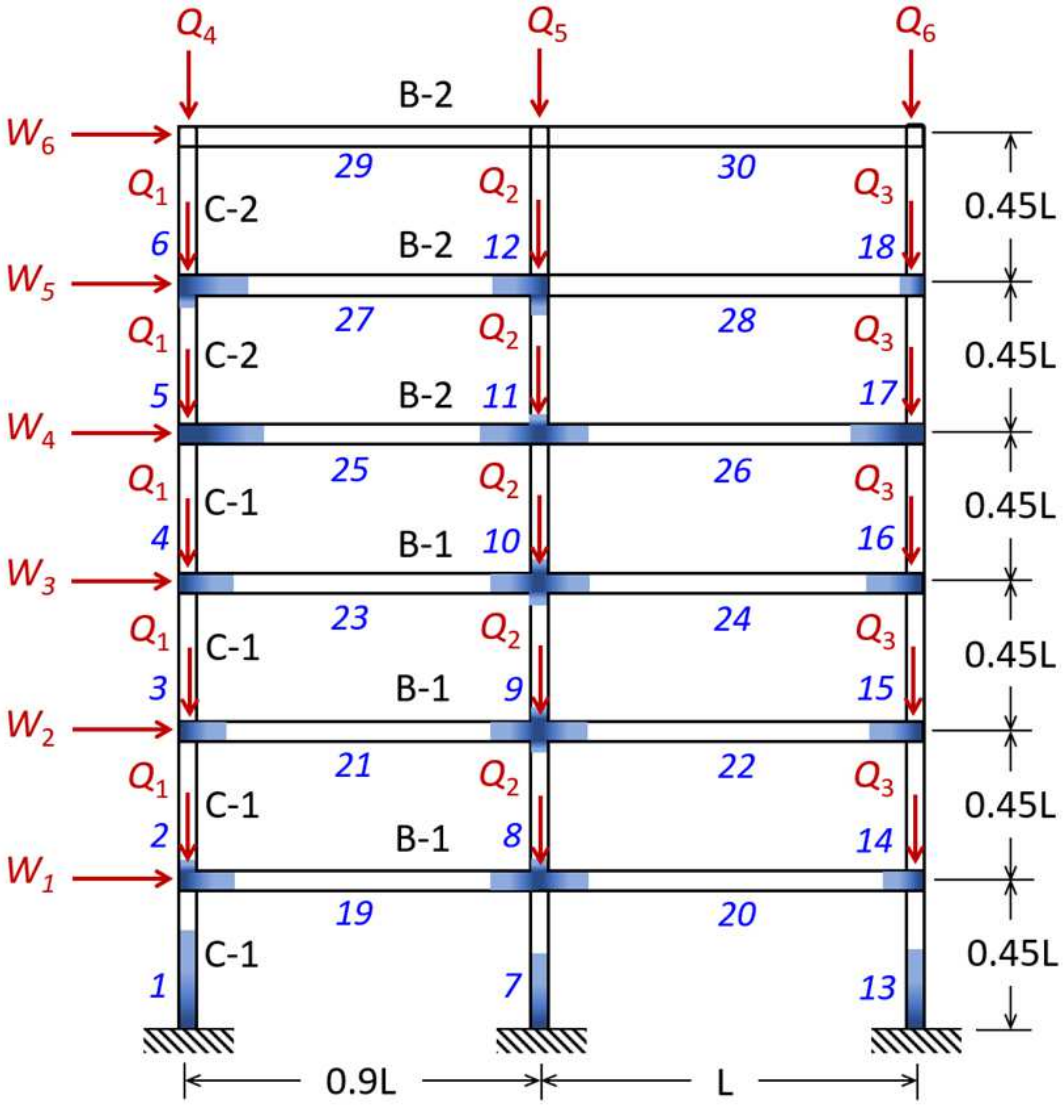

Figure 10: Test Frame 3 model and yielded regions

Table 3: Test Frame 3 member and load information

W-Shape		Gravity Loads (kips)		Lateral Loads (kips)	
B-1	W12x50	Q_1	100	W_1	4
B-2	W12x30	Q_2	60	W_2	8
C-1	W12x79	Q_3	40	W_3	12
C-2	W12x40	Q_4	80	W_4	16
		Q_5	48	W_5	19
		Q_6	32	W_6	24

In Fig. 11, the relative error results are very similar to those found in Figs. 3 and 5 for the two test beam conditions. Comparing the models using 2 elements per member with 100 load increments, the *abc* element model has a relative error of +0.29%, and the *ab* element model has a relative error of +1.14%. The relative errors of the *abc* element models are consistently lower than those of the *ab* element models. This is primarily due to the reduced nonlinear geometric effects of the *abc* element models. The number of load increments does not appreciably affect the accuracy the *abc* element models, but they have a greater effect on the accuracy of the *ab* element models. As with the other test conditions, reducing the number of load increments artificially stiffens the modeled response and the relative errors move downward. Considering the full range of modeling conditions, the *abc* element generally provides superior results over the *ab* element.

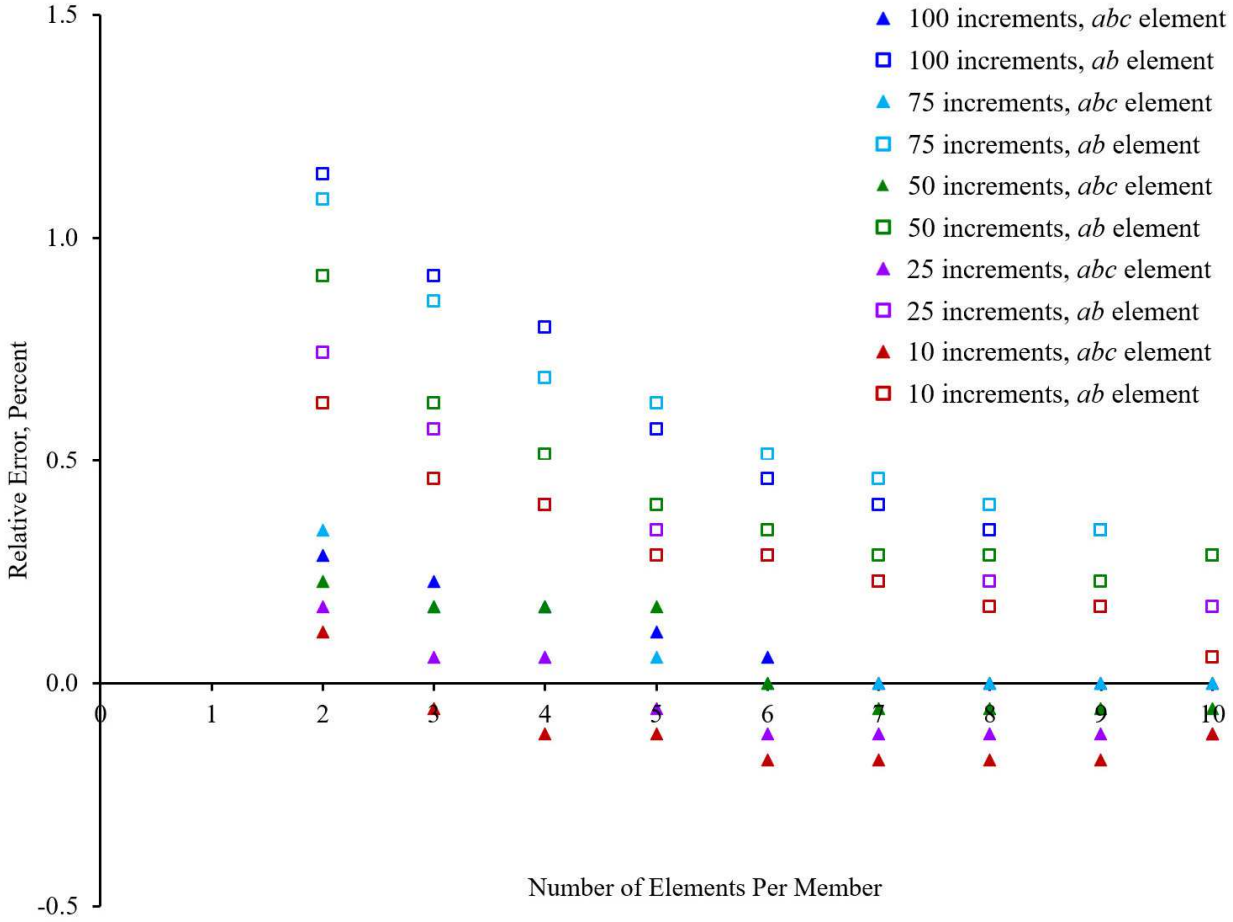

Figure 11: Test Frame 3 relative error results

6. Conclusions

The goals of this research were to develop a new closed-form stiffness matrix that assumes a second-order stiffness reduction over the element length and to assess its ability to consistently provide better results than the previously developed stiffness matrix that assumes a linear stiffness reduction. The following conclusions can be made:

- When determining the modeling conditions for the design of unbraced frames with geometric and material nonlinearities, care must be taken in selecting the element type, increment size,

and number of elements per member, because erroneous decisions can be made if they are based on limited test results with relatively few elements per member and a small number of load increments.

- Based on the relative error comparisons of all five test structures, the *abc* element generally provides superior results over the *ab* element, but a poor choice of load increments and number of elements per member can eliminate its potential benefit.
- Over a wide range of axial force and moment conditions that produce inelastic response, the *abc* element has more stiffness than the *ab* element and decreasing the number of load increments artificially stiffens the modeled response regardless the element type.
- Analyses with 100 load increments revealed that the two test beams modeled using 1 *abc* element per member had relative errors that were 2.0 to 3.4 times lower than when modeled using 1 *ab* element, and the three unbraced frames modeled using 2 *abc* elements per member had relative errors that were 2.6 to 4.0 times lower than when modeled using 2 *ab* elements.

References

MASTAN2, Version 3.5. (2015). Ziemian R.D., McGuire W.

McGuire, W., Gallagher, R. H., & Ziemian, R. D. (2000). *Matrix structural analysis*, 2nd Ed., Wiley, New York.

Rosson, B.T. (2017). "Major and minor axis stiffness reduction of steel beam-columns under axial compression and tension conditions." *Proceedings of the 2019 SSRC Annual Stability Conference*, San Antonio, Texas.

Rosson, B.T. (2018). "Modeling the influence of residual stress on the ultimate load conditions of steel frames." *Proceedings of the 2018 SSRC Annual Stability Conference*, Baltimore, Maryland.

Rosson, B.T, & Ziemian R.D. (2019). Validation study of a new inelastic material model for steel W-shapes. *Proceedings of the 2019 SSRC Annual Stability Conference*, St. Louis, Missouri.

Silva, N.R. (2022). *Development and evaluation of a new beam element for modeling the partially yielded regions of steel W-Shapes*. Master of Science Thesis, Florida Atlantic University, Boca Raton, Florida.

Ziemian, R.D., & McGuire, W. (2002). "Modified tangent modulus approach, a contribution to plastic hinge analysis." *Journal of Structural Engineering*, 128(10), 1301–1307

Zubydan, A.H. (2011). "Inelastic second order analysis of steel frame elements flexed about minor axis." *Engineering Structures*, 33(4), 1240–1250.